Am J Cancer Res 2019;9(5):1061-1073
www.ajcr.us /ISSN:2156-6976/ajcr0092989

Original Article

SSH3 facilitates colorectal cancer cell invasion and metastasis by affecting signaling cascades involving LIMK1/Rac1

Yu-Han Hu[1,2], Yan-Xia Lu[1], Zhe-Ying Zhang[2], Jian-Ming Zhang[1], Wen-Juan Zhang[1], Lin Zheng[1], Wei-Hao Lin[1], Wei Zhang[1], Xue-Nong Li[1]

[1]Department of Pathology, School of Basic Medical Sciences, Southern Medical University, Guangzhou, Guangdong, China; [2]Department of Pathology, School of Basic Medical Sciences, Xinxiang Medical University, Xinxiang, Henan, China

Received February 24, 2019; Accepted April 29, 2019; Epub May 1, 2019; Published May 15, 2019

Abstract: Slingshot phosphatase 3 (SSH3) is a member of the SSH phosphatase family that regulates actin filament dynamics. However, its role in cancer metastasis is relatively unclear compared to that of SSH1. Here, we showed that SSH3 was upregulated in colorectal cancer (CRC). Of note, SSH3 was upregulated in the tumor thrombus and lymph node metastasis compared with that in paired primary CRC tissues. High SSH3 expression was associated with the aggressive phenotype of CRC and may be an independent prognostic factor for the poor survival of patients with CRC. SSH3 significantly enhanced the invasion and metastasis of CRC cells in vitro and in vivo. Moreover, SSH3 regulated the remodeling of actin, which is involved in the cytoskeleton signaling pathway, through its interaction with LIMK1/Rac1 and subsequently promoted CRC cell invasion and metastasis. Our data elucidate an important role for SSH3 in the progression of CRC, and SSH3 may be considered a potential therapeutic target for CRC.

Keywords: SSH3, colorectal cancer, invasion, metastasis, LIMK1, Rac1

Introduction

Colorectal cancer (CRC) is one of the most common digestive malignancies, with high mobility and mortality [1]. It has been demonstrated that invasion and metastasis are the main biological features of malignant tumors, and metastasis is one of the major causes of CRC-related death [2]. However, the mechanisms underlying CRC metastasis are unclear. Therefore, it is important to explore the molecular signatures for the metastatic behavior of CRC cells.

In eukaryotes, the cytoskeleton consists of F-actin, microtubules and intermediate filaments. It is a system of intracellular filaments crucial for cell shape, division, and function in all three domains of life [3]. Previous studies have revealed that the cytoskeleton can change in shape and movement behavior in response to various stimulations anytime and anywhere in tumor cells [4-7]. Abnormal regulation of the cytoskeleton plays an essential role in the metastasis of tumors [8-10].

Slingshot phosphatase 3 (SSH3) is located on chromosome 11q13.2, includes 14 exons, and encodes the SSH3 protein. It is a member of the Slingshot phosphatase family that dephosphorylates and reactivates an inactive ADF/Cofilin [11]. Three members (SSH1, SSH2 and SSH3) comprise the Slingshot phosphatase family. It has been demonstrated that SSH1 is up-regulated in various types of tumors [12, 13], and the upregulation of SSH1 could promote the metastasis of breast cancer [14]. However, the number of investigations of SSH3 is relatively less than that of SSH1. Although it has been revealed that SSH3 is upregulated in circulating cancer cells (CCCs) compared to primary cancer cells (PCCs) in an orthotopic model of breast cancer [15], there is currently less evidence suggesting the function and mechanism of SSH3 in invasion and metastasis.

In this research, we sought to investigate the expression of SSH3 in CRC tissues and cell lines, elucidate its function and explore the molecular mechanisms by which SSH3 promotes invasion and metastasis by regulating

the cytoskeleton signaling pathway in CRC. To some extent, our investigation may help increase the understanding of the mechanisms of invasion and metastasis in CRC, which may assist in the development of new therapeutic strategies for CRC.

Materials and methods

Tissue specimens

All CRC tissues and matched adjacent normal mucosa samples were collected from Nanfang Hospital, Southern Medical University with the informed consent of patients. None of the patients had received radiotherapy or chemotherapy before surgery. The clinical research was performed according to the written approval obtained from the Southern Medical University Institutional Board (Guangzhou, China). In total, 83 CRC tissues and matched adjacent normal mucosa samples were collected between 2012 and 2015. For each tissue, one portion was snap-frozen in liquid nitrogen and stored at -80°C for quantitative real-time PCR (qRT-PCR) and Western blot analyses, and another protion was fixed in 10% formalin within 1 h after surgical removal, embedded in paraffin, and sectioned consecutively at 3 μm thickness using a rotary microtome for immunohistochemical assays. Notably, 35 of the primary CRC tissues were diagnosed with tumor thrombus in the vessels and paired lymph node metastasis. The medical records of 83 patients were reviewed for the acquisition of the following clinicopathological information: age, gender, differentiation, and TNM stage.

Cell cultures

Human CRC cell lines LS174T, HT29, SW620, SW480, DLD-1, RKO, LoVo, Caco2, and HCT116 were obtained from The Global Bioresource Center (ATCC, USA). The cells were cultured in RPMI1640 medium (Gibco) supplemented with 10% fetal bovine serum (FBS) (Gibco) at 37°C in a humidified atmosphere with 5% CO_2.

Real-time quantitative PCR, Western blot, and immunohistochemistry

Real-time quantitative PCR (qRT-PCR), Western blot (WB) and Immunohistochemistry (IHC) were conducted according to previously described methods [16]. Further details are provided in the Supplementary Data Files (Table S1).

Vector construction and retroviral infection

The SSH3 construct was generated by subcloning PCR amplified full-length human SSH3 cDNA into pReceiver-Lv105. For the deletion of SSH3, the shRNA sequence (CCTGCTGGTAGTTTCTACA) was cloned into GV112. Retroviral production and infection were performed as previously described [17]. Stable cell lines expressing SSH3 or shSSH3 were selected for 10 days with 0.5 mg/mL puromycin.

Three-dimensional morphogenesis assay

Twenty-four-well plates were coated with Growth Factor Reduced Matrigel (BD Biosciences). Cells (1×10^4 per well) were suspended in growth medium containing 2% Matrigel and added to the top of the solidified Matrigel. The medium was replaced every 3 to 4 days. The three-dimensional morphological structure was observed by microscopy for 2-3 weeks. The filopodia formed by each cell sphere were counted according to the previous study, and the number of filopodia formed by each cell sphere reflects its invasive ability [18].

Transwell and wound healing assays

The transwell and wound healing assays were conducted as previously described [19]. Further details are provided in the Supplementary Data Files (Supplementary Materials and Methods).

Lung colonization assay

Female athymic BALB/c nude mice (4-6 weeks of age, 18-20 g) were obtained from the Central Laboratory of Animal Science at Southern Medical University and housed in laminar flow cabinets under specific pathogen-free conditions. All experimental procedures involving animals were performed in accordance with animal protocols approved by the Animal Care and Use Committee of Southern Medical University. A total of 2×10^6 cells were injected into the tail veins of nude mice (n = 6 per group); eight weeks later, the mice were sacrificed, and their lungs were removed and formalin fixed for histological analysis [20, 21]. The metastatic tissue was analyzed using hematoxylin and eosin (H&E) staining. The number of metastatic lung nodules in individual mice was counted under a microscope.

Orthotopic mouse metastatic model

A surgical orthotopic implantation mouse model of CRC was established as previously described [17]. A total of 2×10^6 cells were subcutaneously injected into the right dorsal flanks of female BALB/c athymic nude mice. From the seventh day after injection, the size of the tumor was measured as described previously. For orthotopic metastasic assays, nude mice were anesthetized, and their caeca were exteriorized by laparotomy. The subcutaneous tumors were cut into small masses and embedded into the mesentery at the tail end of the caecum. The gut was repositioned to the abdominal cavity and subsequently closed with surgical sutures. Six weeks later, the mice were sacrificed, and all organs were resected for biopsy.

Immunofluorescence analysis

Cells were seeded onto coverslips at a density of 5×10^4 per well for 48 h and then probed with primary antibodies against SSH3 (Proteintech Group, Chicago, MA, USA) and LIMK1 (Abcam, USA) overnight at 4°C. The coverslips were then incubated with rhodamine-conjugated or fluorescein isothiocyanate (FITC)-conjugated goat antibodies against rabbit or mouse IgG (ZSGB-bio, Beijing, China). F-actin was stained with rhodamine-phalloidin. After counterstaining with DAPI (Sigma, St. Louis, MO, USA), images were taken using an Olympus FV1000 confocal laser-scanning microscope (Olympus America Inc, NY, USA). The experiment was performed with three replicates.

Co-immunoprecipitation (Co-IP)

Proteins were extracted from HT29 cells with lysis buffer. SSH3 (Proteintech Group, Chicago, MA, USA), LIMK1 (Abcam, USA) or Rac1 (Abcam, USA) antibodies were added to cell lysates. Subsequently, approximately 30 μl of agarose-protein G beads were added. After incubation for two hours, the beads were washed three times in PBS, and the proteins were eluted in Laemmli buffer. The interacting proteins were analyzed by Western blot.

Statistical analysis

All statistical analyses were performed using SPSS 19.0 for Windows. The differences between groups were examined using one-way ANOVA or a two-tailed Student's t-test. The relationships between SSH3 expression and clinicopathological characteristics were determined using the Mann-Whitney U-test. The survival curve was plotted using the Kaplan Meier method and compared using the log-rank test. Data are presented as the mean ± SD of at least 3 independent experiments. $P < 0.05$ was considered statistically significant.

Results

The upregulation of SSH3 was correlated with advanced progression and a poorer prognosis of CRC

The public database Oncomine (https://www.oncomine.org) and GEO datasets (GSE24551 and GSE41258) were utilized to examine the expression of SSH3 in CRC tissues. SSH3 was upregulated in CRC, especially in liver metastasis compared to the primary tumor (Supplementary Data File: Figure S1A, S1B). Consistent with this result, the expression of SSH3 was higher in 29 of 32 CRC tissues compared to their adjacent normal mucosa tissues using qRT-PCR (**Figure 1A**). An increase in SSH3 expression was also observed by Western blot analysis in the same samples (**Figure 1B**). The expression levels of SSH3 were also examined in 83 CRC tissues using IHC. 35 of these samples were diagnosed with an endovascular tumor thrombus and lymph node metastasis. SSH3 was upregulated in the endovascular tumor thrombus and lymph node metastasis compared with the primary CRC tissues, in which SSH3 was overexpressed compared to their adjacent normal mucosa tissues (**Figure 1C**, **1E**). Correlation analysis showed that increased SSH3 expression was significantly correlated with poorer tumor differentiation, advanced TNM stage, and metastasis (**Figure 1C**, **1D**; **Tables 1**, **2**). Kaplan Meier survival analyses published in PROGgene (http://www.compbio.iupui.edu/proggene) revealed that higher expression levels of SSH3 were significantly correlated with poor patient survival (**Figure 1F**). These results suggest that SSH3 may be a prognostic biomarker for CRC.

Upregulation of SSH3 promotes the invasion and metastasis of CRC cells, and exogenous SSH3 knockdown inhibits the invasion and metastasis of CRC cells

The expression of SSH3 was examined in different CRC cells (Supplementary Data File: Figure

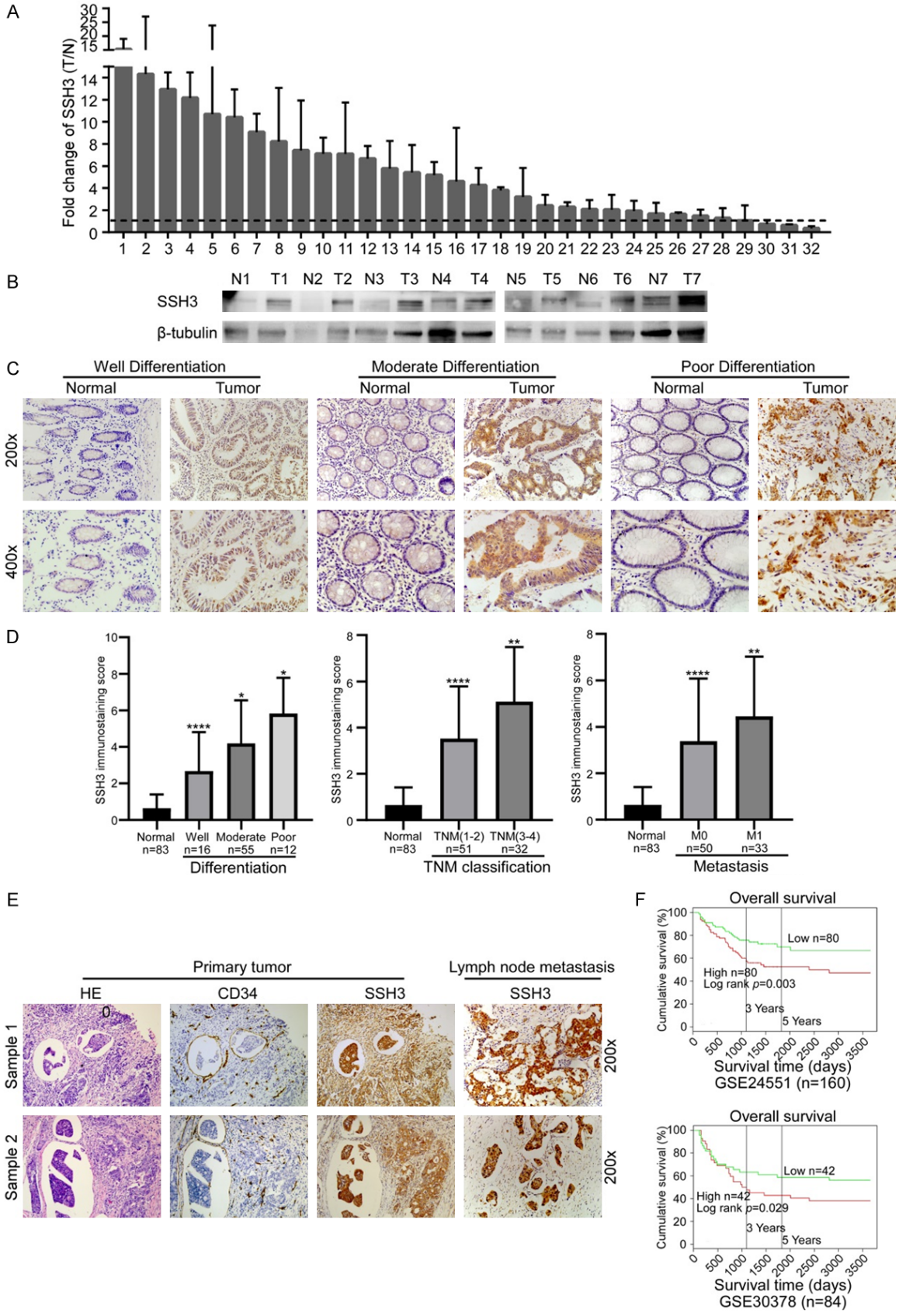
A
Fold change of SSH3 (T/N)
B
N1 T1 N2 T2 N3 T3 N4 T4 N5 T5 N6 T6 N7 T7
SSH3
β-tubulin
C
Well Differentiation
Moderate Differentiation
Poor Differentiation
Normal
Tumor
200x
400x
D
SSH3 immunostaining score
Normal n=83
Well n=16
Moderate n=55
Poor n=12
Differentiation
TNM(1-2) n=51
TNM(3-4) n=32
TNM classification
M0 n=50
M1 n=33
Metastasis
E
Primary tumor
Lymph node metastasis
HE
CD34
SSH3
Sample 1
Sample 2
200x
F
Overall survival
Cumulative survival (%)
Low n=80
High n=80
Log rank p=0.003
3 Years
5 Years
Survival time (days)
GSE24551 (n=160)
Low n=42
High n=42
Log rank p=0.029
GSE30378 (n=84)

Figure 1. Expression of SSH3 in CRC and its correlation with CRC prognosis. A. qRT-PCR analysis of SSH3 expression in 32 paired CRC tissues; SSH3 was quantified relative to the matched adjacent no tumor tissues. Error bars represent means ± SD calculated from three parallel experiments. B. Expression analyses of SSH3 protein in 7 surgical CRC tissues and the paired normal intestine epithelial samples using Western blot. β-tubulin was used as a loading control. C. Immunostaining of SSH3 protein in CRC tissue samples and normal colorectal tissues. D. Statistical analyses of the average SSH3 immunostaining score between normal intestinal tissues and CRC specimens with different degrees of differentiation, TNM classification and Metastasis (*$P < 0.05$, **$P < 0.01$, ***$P < 0.001$, ****$P < 0.0001$). E. Immunostaining of SSH3 protein in CRC tissue samples diagnosed with tumor thrombus and the paired lymph node metastasis. F. Kaplan-Meier survival analyses published in PROG gene revealed that a higher expression of SSH3 was significantly correlated with poorer survival of patients.

Table 1. The relationship between the expression of SSH3 and clinicopathological parameters

Clinicopathological variables	SSH3 expression		Z	*p* value
	High	Low		
Age				
≤ mean (58)	18	20	-0.538	0.590
> mean (58)	24	21		
Gender				
Male	25	21	-0.756	0.449
Female	17	20		
Differentiation				
Well	6	10	-2.609	0.009
Moderate	25	30		
Poor	11	1		
TNM classification				
I-II	21	30	-2.155	0.031
III-IV	21	11		
Metastasis				
No	20	30	-2.364	0.018
Yes	22	11		

Table 2. Spearman correlation analysis between the expression of SSH3 and Clinicopathological Features

Variables	SSH3 expression	
	Spearman correlation	*p* value
Age	-0.075	0.500
Gender	-0.032	0.772
Differentiation	0.220	0.045
TNM	0.222	0.044
Metastasis	0.219	0.047

S2). SSH3 was stably expressed in SW480 and SW620 cells, generating subcell lines SW480-SSH3 and SW620-SSH3, respectively, and their controls were infected with lentiviruses containing empty vectors (**Figure 2A**). Correspondingly, SSH3 was permanently knocked down in HT29 and HCT116 cells by the shSSH3 lentiviruses, producing the HT29-shSSH3 and HCT116-shSSH3 subcell lines, respectively, and scramble was used as a control (**Figure 3A**). The three-dimensional morphogenesis analysis showed that forced SSH3 expression led to a marked increase in the number of protrusions in SW480 and SW620 cells (**Figure 2B**). Accordingly, the upregulation of SSH3 promoted cell migration compared with that in control cells, as measured by transwell migration and wound healing assays (**Figure 2C**, **2D**). However, reducing SSH3 in CRC cell lines yielded the opposite effects (**Figure 3B-D**).

Moreover, we injected SW480-SSH3 or HT-29-shSSH3 cells and their control cells into nude mice via the tail vein to observe the effect of SSH3 on the potential of homing capacity. SSH3 significantly increased the lung homing capacity of SW480 cells compared with the effect of the vector (**Figure 4A**, **4B**). However, fewer tumor nodules were formed in the lungs of the SSH3 knockdown group (**Figure 4C**, **4D**). In addition, tiny tumor masses of subcutaneous tumors were transplanted into the mouse cecal subserosa. The number of hepatic metastatic lesions in the mice of the SW480-SSH3 group was obviously increased compared with that of the control group (**Figure 4E**, **4F**). In particular, the expression of SSH3 was higher in the tumor thrombus than in the primary tumor in the mouse mucosa (Supplementary Data File: Figure S3), which was consistent with the expression of SSH3 in human CRC tissues.

High SSH3 expression promotes the invasion and metastasis of CRC cells by regulating the cytoskeleton

Using GSEA (Gene Set Enrichment Analysis), we found an enrichment of cytoskeleton signaling pathway gene signatures (GSE13067 and GSE17538; **Figure 5A**) with high SSH3 expression.

Next, we explored the colocalization of SSH3 and F-actin in CRC cells. The results showed that the colocalization of SSH3 and F-actin

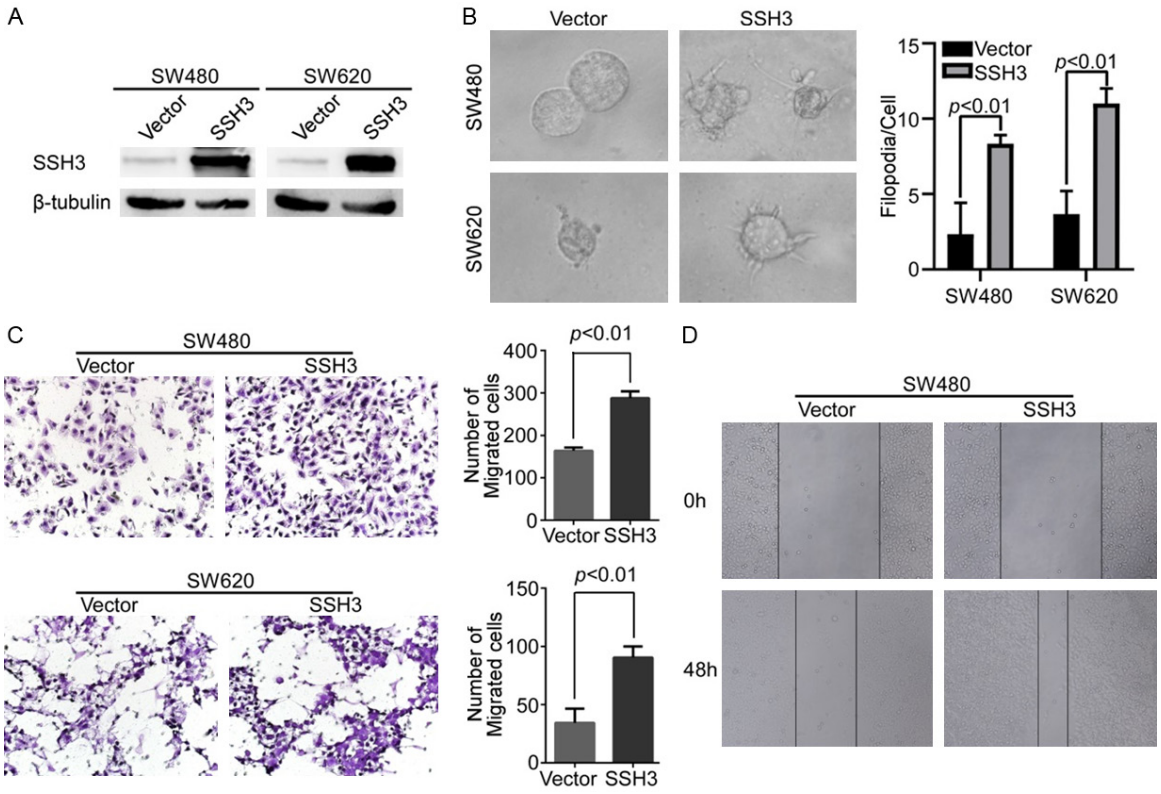

Figure 2. Up-regulation of SSH3 promoted the invasion and metastasis of CRC cell in vitro. A. Overexpression of SSH3 in SW480 and SW620 cells analyzed through Western blot. β-tubulin was used as a loading control. B. The overexpression of SSH3 lead to a marked increase in the number of protrusions in SW480 and SW620 cells in three-dimensional morphogenesis assays. The bar chart represents the filopodia/cell. Error bars represent the means ± SD calculated from three parallel experiments. C. Overexpression of SSH3 increased cell migration as determined by transwell assays. The bar chart represents the migration cell numbers. Error bars represent the means ± SD of 5 different fields. D. Wound healing assay used to determine the migration ability of cells with up-regulated SSH3.

existed in the cytoplasm of HT29 and HCT116 cells (**Figure 5B**). We also observed changes in the cytoskeleton in CRC cells when SSH3 was up- or downregulated. The actin cytoskeletons were reorganized when SSH3 was upregulated (**Figure 5C**), and the cytoskeletons disappeared when SSH3 was downregulated (**Figure 5D**).

SSH3 is involved in the cytoskeleton signaling pathway by interacting with LIMK1 and Rac1

To explore the molecular mechanisms underlying SSH3 in cell cytoskeleton regulation, we analyzed the potential proteins interacting with SSH3 using the public database PrePPI (http://bhapp.c2b2.columbia.edu/PrePPI) and found that LIMK1 is a candidate protein that may interact with SSH3 (Supplementary Data File: Figure S4A).

Pull-down assays were used to identify the SSH3 interacting proteins. The two most obvious pull-down bands identified by mass spectrometry (MS) were LIMK1 and Rac1 when (Supplementary Data File: Figure S4B, S4C). The immunofluorescent colocalization of SSH3 with LIMK1 was observed in CRC cells (**Figure 6A**).

We performed Co-Immunoprecipitation (Co-IP) experiments and determined that SSH3, LIMK1 and Rac1 interact with each other (**Figure 6B**). The upregulation of SSH3 evidently inhibited the phosphorylation levels of LIMK1 and Cofilin (p-LIMK1 and p-Cofilin) (**Figure 6C**). Conversely, the downregulation of SSH3 increased LIMK1 and Cofilin phosphorylation (**Figure 6C**). These results suggest that SSH3 may promote the invasion and metastasis of CRC cells by interacting with LIMK1 and Rac1, which modulate the activity of Cofilin and the rearrangement of the cytoskeleton.

Discussion

Cellular movement in cancer cells is a fundamental biological behavior that contributes to

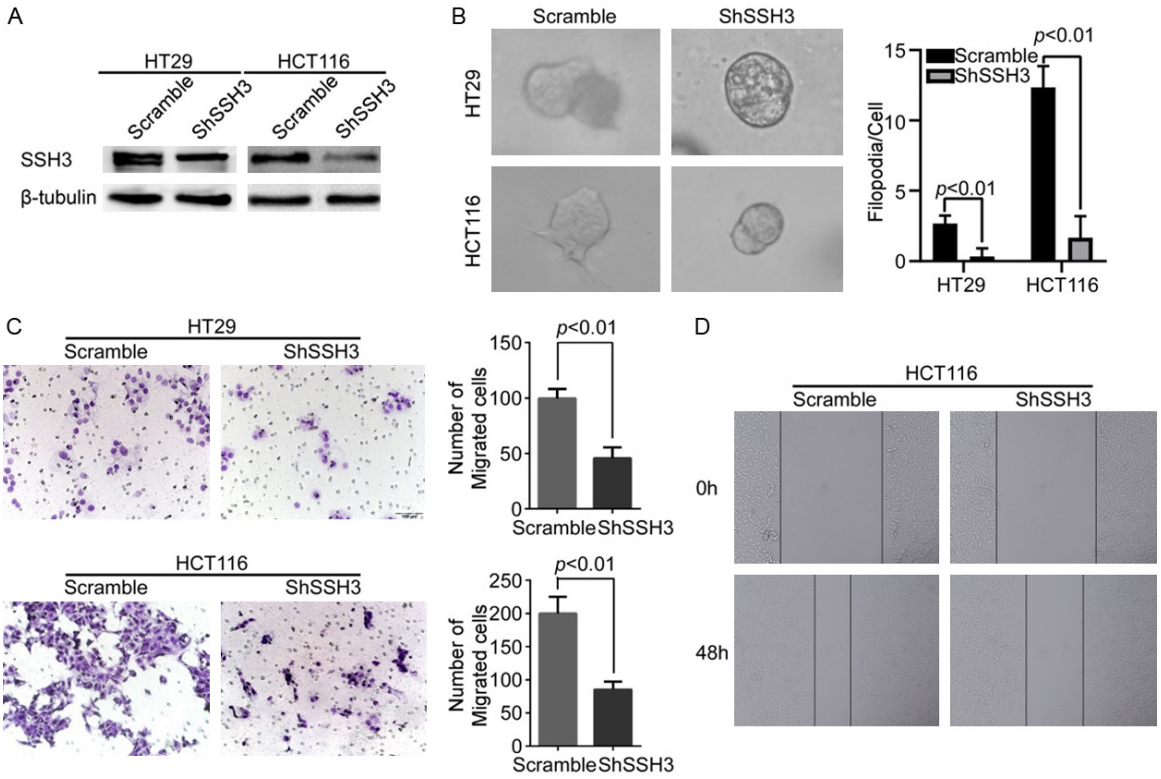

Figure 3. Down-regulation of SSH3 inhibited the invasion and metastasis of CRC cell in vitro. A. Silencing of SSH3 in shRNA-transduced stable HT29 and HCT116 cells. β-tubulin was used as a loading control. B. Reduction of endogenous SSH3 lead to a marked decrease in the number of protrusions in three-dimensional morphogenesis assays. The bar chart represents the filopodia/cell. Error bars represent the means ± SD calculated from three parallel experiments. C. Down-regulation of SSH3 decreased cell migration as determined by transwell assays. The bar chart represents the migration cell numbers. Error bars represent the means ± SD of 5 different fields. D. Wound healing assay used to determine the migration ability of cells with down-regulated SSH3.

invasion and metastasis. Actin protein and its regulatory protein, as basic engines for cellular mobility, play a critical role in the migration and metastasis of cancer cells [22]. Dynamic regulation of the actin strand is essential for cell migration and invasion [23]. The SSH family appears to play a role in actin dynamics by reactivating ADF/Cofilin proteins in vivo. It is well established that SSH1 contributes to actin remodeling by dephosphorylating and activating the actin-severing protein Cofilin [24]. However, there is no obvious evidence showing that SSH3 modulates actin dynamics. In the current work, we found that SSH3 was upregulated in the endovascular tumor thrombus and lymph node metastasis compared with the primary CRC tissues, in which SSH3 was overexpressed comparing to their paired normal mucosa tissues. Increased SSH3 expression was significantly associated with the aggressive cellular characteristics of CRC (e.g., poor differentiation and advanced TNM stage) and a poor outcome of patients, suggesting that SSH3 might be a tumor promoter and a prognostic marker of CRC progression. Analyses of Oncomine and the GEO datasets (GSE24551 and GSE41258) showed that SSH3 was upregulated in CRC, especially in liver metastasis compared to that in the primary tumor. Moreover, gene expression microarray analyses revealed that the expression of SSH3 was higher in the circulating cancer cells (CCCs) compared with the primary cancer cells (PCCs) in mice with 4T1 orthotopic tumors [15]. All of the analyses suggested that the overexpression of SSH3 might facilitate cancer progression and metastasis. Here, we demonstrated that the overexpression of SSH3 significantly enhanced the invasion and metastasis of CRC cells in vitro and in vivo. Moreover, the abnormal expression of SSH3 changed the cytoskeleton in CRC cells.

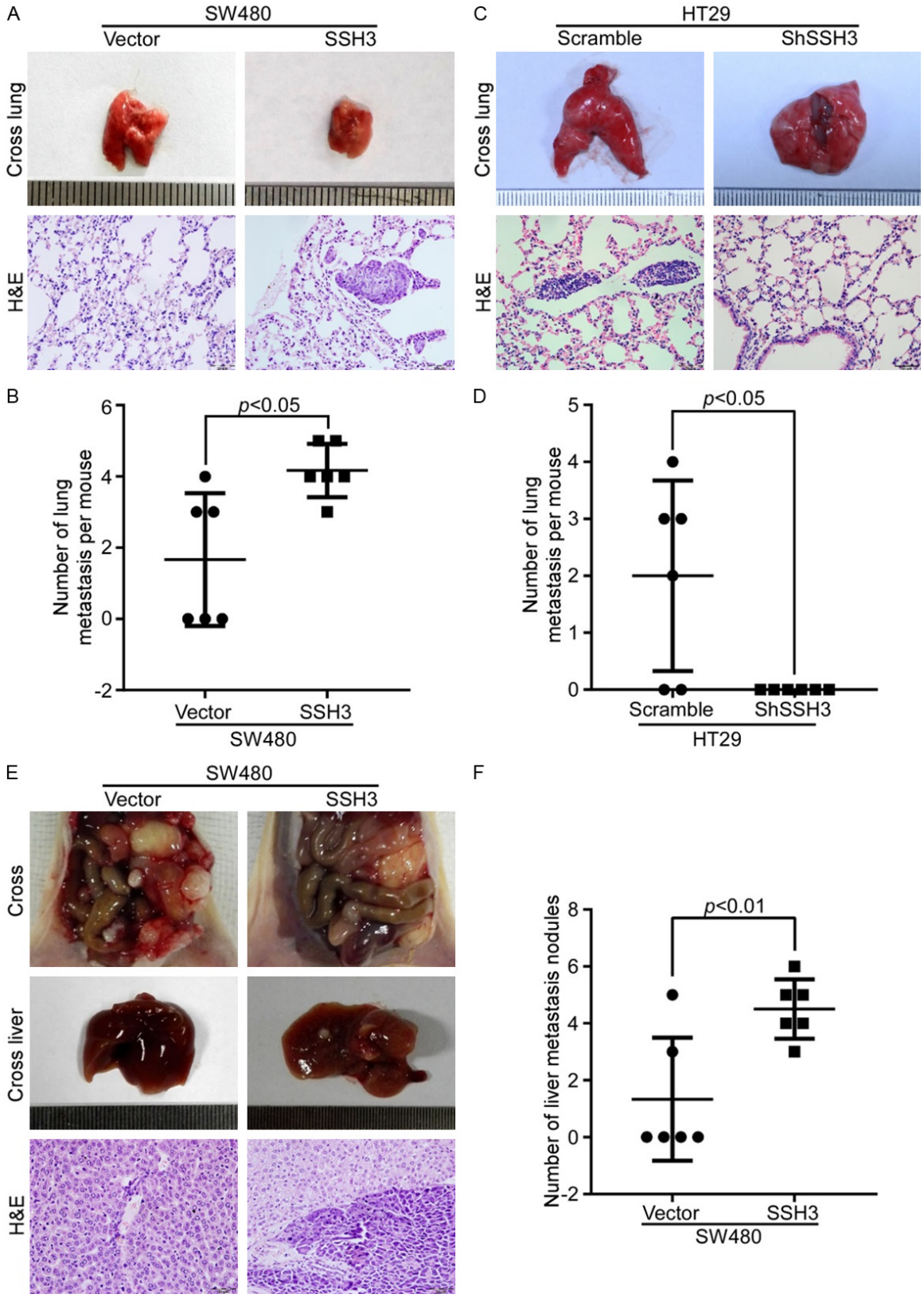

Figure 4. SSH3 promotes the metastatic potential of CRC cells in vivo. A and C. The representative gross images of the lungs from different experimental groups are shown. Sections of the liver were stained with H&E. B and D. Box-scatter plots show the number of metastatic nodules in the lungs as observed in each group. E. The representative gross images of the intestines and livers from different experimental groups are shown. Sections of the liver were stained with H&E. F. Box-scatter plot shows the number of metastatic nodules in the liver as observed in each group.

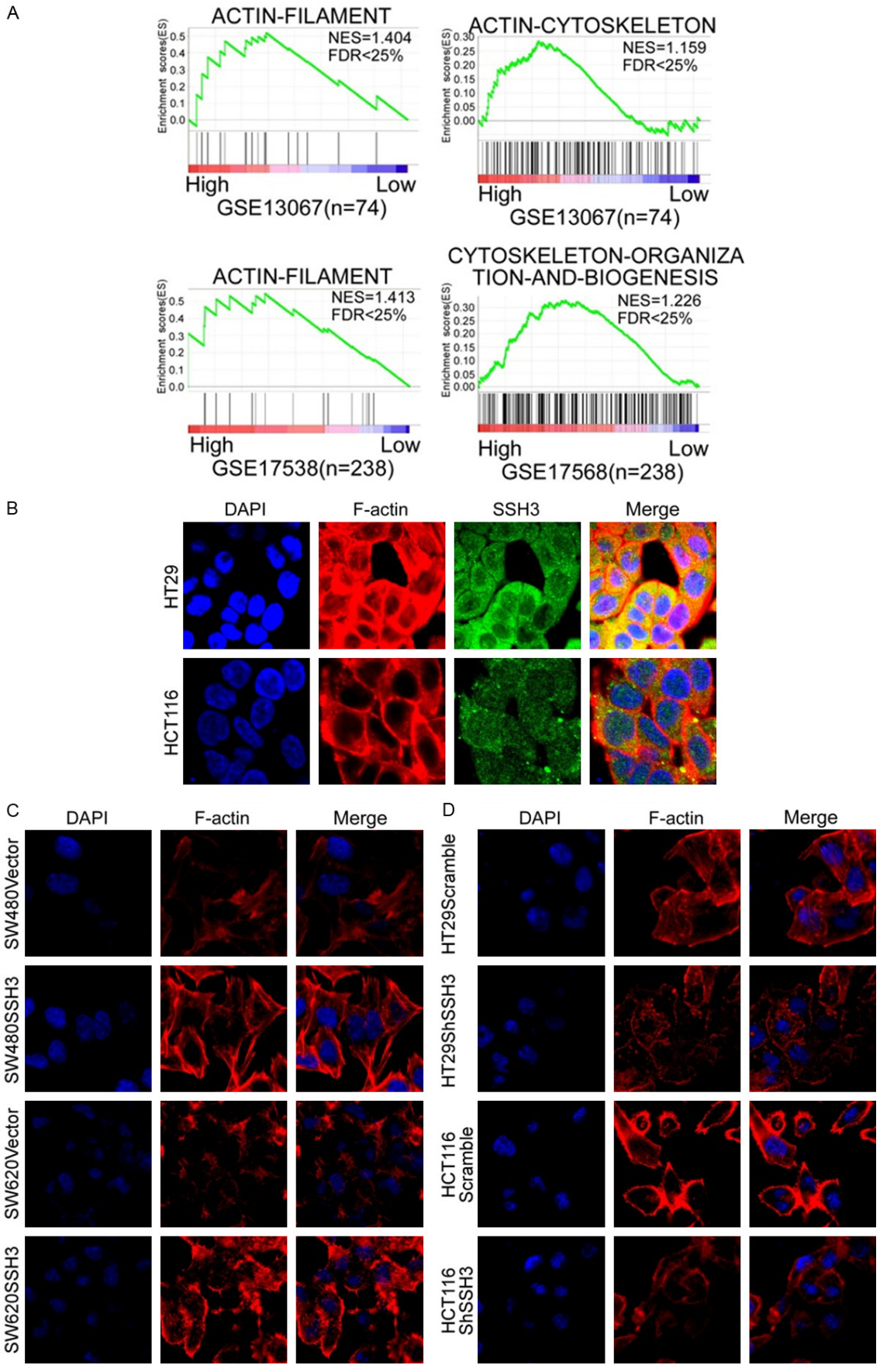
A
ACTIN-FILAMENT
NES=1.404
FDR<25%
Enrichment scores(ES)
High
Low
GSE13067(n=74)
ACTIN-CYTOSKELETON
NES=1.159
FDR<25%
GSE13067(n=74)
ACTIN-FILAMENT
NES=1.413
FDR<25%
GSE17538(n=238)
CYTOSKELETON-ORGANIZATION-AND-BIOGENESIS
NES=1.226
FDR<25%
GSE17568(n=238)
B
DAPI
F-actin
SSH3
Merge
HT29
HCT116
C
SW480Vector
SW480SSH3
SW620Vector
SW620SSH3
D
HT29Scramble
HT29ShSSH3
HCT116 Scramble
HCT116 ShSSH3

Figure 5. High expression of SSH3 promotes the invasion and metastasis of CRC cells by regulating the cytoskeleton. A. Analyses of SSH3-regulated gene signatures via GSEA. B. Co-localization of SSH3 and F-actin in CRC cells. C and D. Rearrangements of cytoskeleton in CRC cells when SSH3 was up- or downregulated.

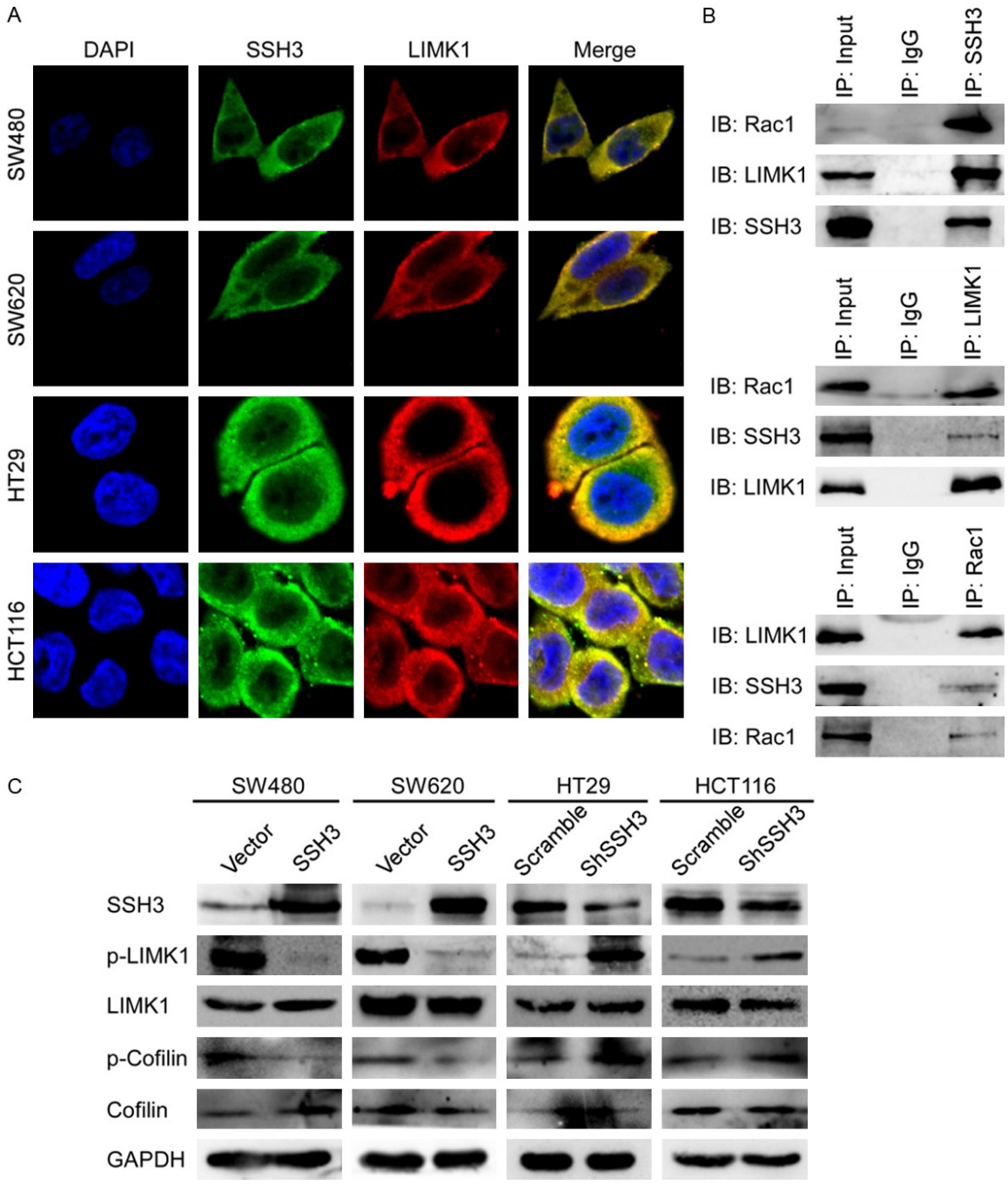

Figure 6. SSH3 is involved in the cytoskeleton signaling pathway by interacting with LIMK1 and Rac1. A. Colocalization of SSH3 and LIMK1 in CRC cells. B. Extracts of HT29 cells were subjected to Co-IP using SSH3 antibody or control IgG, and Western blot was performed with LIMK1 and Rac1 antibodies. Reciprocal Co-IPs were performed using LIMK1, Rac1 and IgG antibodies, followed by Western blot with SSH3, Rac1 or LIMK1 antibodies. C. Expression of LIMK1, p-LIMK1, Cofilin and p-Cofilin when SSH3 was up-regulated or down-regulated using Western blot. GAPDH was using as a loading control.

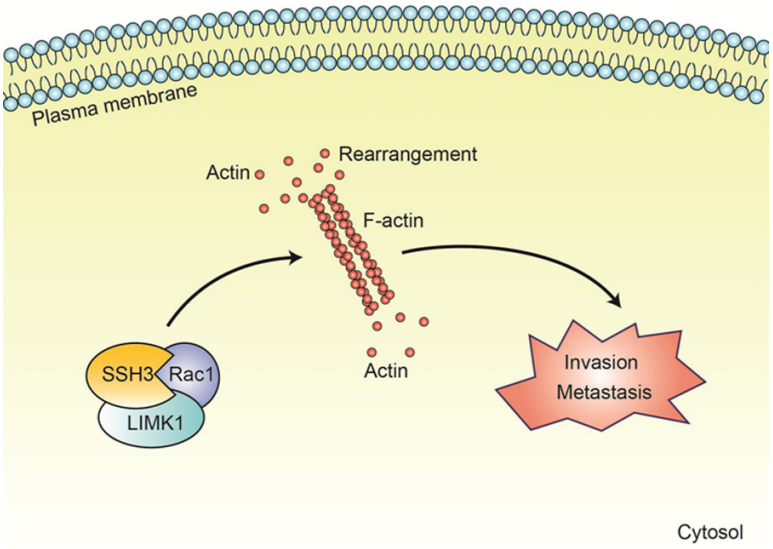

Figure 7. A model of SSH3 involvement in CRC. SSH3 may promote the invasion and metastasis of CRC by interacting with LIMK1 and Rac1 which can modulate the activity of Cofilin and the rearrangements of cytoskeleton.

However, the relationships and molecular mechanisms through which SSH3 interacts with actin dynamics remain unknown. Bioinformatic and mass spectrometry (MS) analyses suggested that the candidate proteins interacting with SSH3 may be LIMK1 and Rac1.

LIMK1 (LIM motif-containing protein kinase-1) is a kinase that contains 2 N-terminal LIM motifs and a C-terminal protein kinase domain [25, 26], phosphorylating the Ser3 of Cofilin directly, causing the inactivation of Cofilin and regulating actin polymerization [26-28]. Studies have demonstrated that the spatial and temporal regulation of Cofilin activity by LIM kinase and Slingshot is critical for directional cell migration [29]. Our present study also revealed that the colocalization of SSH3 and LIMK1 existed in CRC cells, and LIMK1 and Cofilin can be dephosphorylaed by SSH3. Therefore, it is perhaps not surprising that SSH3 may play central roles in invasion and metastasis by modulating actin dynamics.

Rac1 is a member of the Rho GTPase family which includes small GTP-binding proteins [30, 31]. Rac1 is identified as a crucial regulator of actin cytoskeleton dynamics. Activated Rac1 can facilitate actin polymerization at the cell periphery to stimulate the formation of pseudopods [32]. Rac1 has been suggested to activate p21-activated kinases (PAKs), and the activation of PAKs is a regular manner for increasing cell motility. Active PAKs greatly enhance the phosphorylation and activation of LIMK1, and activated LIMK1 further exerts its effects on the architecture of the actin cytoskeleton by phosphorylating and regulating the activity of Cofilin proteins, resulting in the growth of actin filaments [33]. Our results showed that SSH3, LIMK1 and Rac1 can interact with each other. The interactions between SSH3, LIMK1 and Rac1 suggest that some functional coregulation might be involved.

We speculate that the functional coregulation of SSH3, LIMK1 and Rac1 may cause the rapid turnover of the cytoskeleton, and ultimately promote the invasion and metastasis of CRC (**Figure 7**). However, the underlying mechanism still needs further study.

Combining the results of our present study with other results from the literature led us to propose a working model in which SSH3 promotes colorectal cancer cell invasion and metastasis by affecting signaling cascades involving LIMK1/Rac1.

Acknowledgements

This work was supported by the National Natural Science Foundation of China (No. 8167-2429, No. 81874074 and No. 81502479).

Disclosure of conflict of interest

None.

Address correspondence to: Xue-Nong Li, Department of Pathology, School of Basic Medical Sciences, Southern Medical University, Guangzhou, Guangdong, China. Tel: +86-20-6164-8720; Fax: +86-20-6164-8720; E-mail: nfydlxn@126.com

References

[1] Siegel RL, Miller KD and Jemal A. Cancer statistics, 2017. CA Cancer J Clin 2017; 67: 7-30.

[2] Chaffer CL and Weinberg RA. A perspective on cancer cell metastasis. Science 2011; 331: 1559-1564.

[3] Wickstead B and Gull K. The evolution of the cytoskeleton. J Cell Biol 2011; 194: 513-525.
[4] Raftopoulou M and Hall A. Cell migration: Rho GTPases lead the way. Dev Biol 2004; 265: 23-32.
[5] Chan CK, Pan Y, Nyberg K, Marra MA, Lim EL, Jones SJ, Maar D, Gibb EA, Gunaratne PH, Robertson AG and Rowat AC. Tumour-suppressor microRNAs regulate ovarian cancer cell physical properties and invasive behaviour. Open Biol 2016; 6.
[6] Dinicola S, Fabrizi G, Masiello MG, Proietti S, Palombo A, Minini M, Harrath AH, Alwasel SH, Ricci G, Catizone A, Cucina A and Bizzarri M. Inositol induces mesenchymal-epithelial reversion in breast cancer cells through cytoskeleton rearrangement. Exp Cell Res 2016; 345: 37-50.
[7] Zhan H, Ma J, Ruan F, Bedaiwy MA, Peng B, Wu R and Lin J. Elevated phosphatase of regenerating liver 3 (PRL-3) promotes cytoskeleton reorganization, cell migration and invasion in endometrial stromal cells from endometrioma. Hum Reprod 2016; 31: 723-733.
[8] Huang D, Cao L and Zheng S. CAPZA1 modulates EMT by regulating actin cytoskeleton remodelling in hepatocellular carcinoma. J Exp Clin Cancer Res 2017; 36: 13.
[9] Liu Y, Wang Z, Huang D, Wu C, Li H, Zhang X, Meng B, Li Z, Zhu T, Yang S and Sun W. LMO2 promotes tumor cell invasion and metastasis in basal-type breast cancer by altering actin cytoskeleton remodeling. Oncotarget 2017; 8: 9513-9524.
[10] Kazazian K, Go C, Wu H, Brashavitskaya O, Xu R, Dennis JW, Gingras AC and Swallow CJ. Plk4 promotes cancer invasion and metastasis through Arp2/3 complex regulation of the actin cytoskeleton. Cancer Res 2017; 77: 434-447.
[11] Niwa R, Nagata-Ohashi K, Takeichi M, Mizuno K and Uemura T. Control of actin reorganization by Slingshot, a family of phosphatases that dephosphorylate ADF/cofilin. Cell 2002; 108: 233-246.
[12] Maimaiti Y, Maimaitiming M, Li Y, Aibibula S, Ainiwaer A, Aili A, Sun Z and Abudureyimu K. SSH1 expression is associated with gastric cancer progression and predicts a poor prognosis. BMC Gastroenterol 2018; 18: 12.
[13] Aggelou H, Chadla P, Nikou S, Karteri S, Maroulis I, Kalofonos HP, Papadaki H and Bravou V. LIMK/cofilin pathway and Slingshot are implicated in human colorectal cancer progression and chemoresistance. Virchows Arch 2018; 472: 727-737.
[14] Wang LH, Xiang J, Yan M, Zhang Y, Zhao Y, Yue CF, Xu J, Zheng FM, Chen JN, Kang Z, Chen TS, Xing D and Liu Q. The mitotic kinase Aurora-A induces mammary cell migration and breast cancer metastasis by activating the Cofilin-F-actin pathway. Cancer Res 2010; 70: 9118-9128.
[15] LeBleu VS, O'Connell JT, Gonzalez Herrera KN, Wikman H, Pantel K, Haigis MC, de Carvalho FM, Damascena A, Domingos Chinen LT, Rocha RM, Asara JM and Kalluri R. PGC-1alpha mediates mitochondrial biogenesis and oxidative phosphorylation in cancer cells to promote metastasis. Nat Cell Biol 2014; 16: 992-1003, 1001-1015.
[16] Hu YH, Chen Q, Lu YX, Zhang JM, Lin C, Zhang F, Zhang WJ, Li XM, Zhang W and Li XN. Hypermethylation of NDN promotes cell proliferation by activating the Wnt signaling pathway in colorectal cancer. Oncotarget 2017; 8: 46191-46203.
[17] Lu YX, Yuan L, Xue XL, Zhou M, Liu Y, Zhang C, Li JP, Zheng L, Hong M and Li XN. Regulation of colorectal carcinoma stemness, growth, and metastasis by an miR-200c-Sox2-negative feedback loop mechanism. Clin Cancer Res 2014; 20: 2631-2642.
[18] Ye YP, Jiao HL, Wang SY, Xiao ZY, Zhang D, Qiu JF, Zhang LJ, Zhao YL, Li TT, Li L, Liao WT and Ding YQ. Hypermethylation of DMTN promotes the metastasis of colorectal cancer cells by regulating the actin cytoskeleton through Rac1 signaling activation. J Exp Clin Cancer Res 2018; 37: 299.
[19] Yuan L, Zhou C, Lu Y, Hong M, Zhang Z, Zhang Z, Chang Y, Zhang C and Li X. IFN-gamma-mediated IRF1/miR-29b feedback loop suppresses colorectal cancer cell growth and metastasis by repressing IGF1. Cancer Lett 2015; 359: 136-147.
[20] Zhang Z, Zhou C, Chang Y, Zhang Z, Hu Y, Zhang F, Lu Y, Zheng L, Zhang W, Li X and Li X. Long non-coding RNA CASC11 interacts with hnRNP-K and activates the WNT/beta-catenin pathway to promote growth and metastasis in colorectal cancer. Cancer Lett 2016; 376: 62-73.
[21] Shen Z, Zhou R, Liu C, Wang Y, Zhan W, Shao Z, Liu J, Zhang F, Xu L, Zhou X, Qi L, Bo F, Ding Y and Zhao L. MicroRNA-105 is involved in TNF-alpha-related tumor microenvironment enhanced colorectal cancer progression. Cell Death Dis 2017; 8: 3213.
[22] Rajakyla EK and Vartiainen MK. Rho, nuclear actin, and actin-binding proteins in the regulation of transcription and gene expression. Small GTPases 2014; 5: e27539.
[23] Steinbacher T and Ebnet K. The regulation of junctional actin dynamics by cell adhesion receptors. Histochem Cell Biol 2018; 150: 341-350.
[24] Wang Y, Kuramitsu Y, Kitagawa T, Baron B, Yoshino S, Maehara S, Maehara Y, Oka M and Nakamura K. Cofilin-phosphatase slingshot-1L (SSH1L) is over-expressed in pancreatic can-

cer (PC) and contributes to tumor cell migration. Cancer Lett 2015; 360: 171-176.
[25] Mizuno K, Okano I, Ohashi K, Nunoue K, Kuma K, Miyata T and Nakamura T. Identification of a human cDNA encoding a novel protein kinase with two repeats of the LIM/double zinc finger motif. Oncogene 1994; 9: 1605-1612.
[26] Yang N, Higuchi O and Mizuno K. Cytoplasmic localization of LIM-kinase 1 is directed by a short sequence within the PDZ domain. Exp Cell Res 1998; 241: 242-252.
[27] Arber S, Barbayannis FA, Hanser H, Schneider C, Stanyon CA, Bernard O and Caroni P. Regulation of actin dynamics through phosphorylation of cofilin by LIM-kinase. Nature 1998; 393: 805-809.
[28] Yang N, Higuchi O, Ohashi K, Nagata K, Wada A, Kangawa K, Nishida E and Mizuno K. Cofilin phosphorylation by LIM-kinase 1 and its role in Rac-mediated actin reorganization. Nature 1998; 393: 809-812.
[29] Nishita M, Tomizawa C, Yamamoto M, Horita Y, Ohashi K and Mizuno K. Spatial and temporal regulation of cofilin activity by LIM kinase and Slingshot is critical for directional cell migration. J Cell Biol 2005; 171: 349-359.
[30] Nobes C and Hall A. Regulation and function of the Rho subfamily of small GTPases. Curr Opin Genet Dev 1994; 4: 77-81.
[31] Hall A. Rho family GTPases. Biochem Soc Trans 2012; 40: 1378-1382.
[32] Fort L, Batista JM, Thomason PA, Spence HJ, Whitelaw JA, Tweedy L, Greaves J, Martin KJ, Anderson KI, Brown P, Lilla S, Neilson MP, Tafelmeyer P, Zanivan S, Ismail S, Bryant DM, Tomkinson NCO, Chamberlain LH, Mastick GS, Insall RH and Machesky LM. Fam49/CYRI interacts with Rac1 and locally suppresses protrusions. Nat Cell Biol 2018; 20: 1159-1171.
[33] Tong H, Qi D, Guan X, Jiang G, Liao Z, Zhang X, Chen P, Li N and Wu M. c-Abl tyrosine kinase regulates neutrophil crawling behavior under fluid shear stress via Rac/PAK/LIMK/cofilin signaling axis. J Cell Biochem 2018; 119: 2806-2817.

Supplementary materials and methods

RNA extraction and qRT-PCR

Total RNA was extracted using TRIzol reagent (Takara) according to the manufacturer's instructions. cDNAs were synthesized using a Reverse Transcription Kit (Takara). Quantitative real-time PCR was carried out using SYBR Green I (Takara) in triplicate. The results were normalized to the expression of GAPDH. The primer sequences used for qRT-PCR are listed in Table S1. Relative quantification of mRNA expression was calculated using the $2^{-\Delta\Delta Ct}$ method.

Western blot assay (WB)

Protein lysates were prepared and quantified by a bicinchoninic acid (BCA) protein assay (KeyGen Biotech). Equivalent amounts of protein lysates were separated using 10% SDS-PAGE and transferred onto a PVDF membrane. Then, the membrane was incubated with the primary antibody at 4°C overnight, followed by the appropriate second antibody. The bands were visualized by Pierce ECL Western Blotting Substrate (Thermo Scientific).

Immunohistochemistry (IHC)

The 3 μm-thick tissue sections were deparaffinized and rehydrated, and incubated with primary antibody at 4°C overnight. Prior to incubation with anti-SSH3 (1:100 dilution; Proteintech Group, Chicago, MA, USA), and anti-Ki67 antibodies (1:100 dilution; Bioworld Technology Inc., St. Louis Park, MN, USA), the sections were heated in 0.01 M sodium citrate buffer, pH 6.0 for antigen retrieval, and incubated in 3% H_2O_2 to inhibit endogenous peroxidase activity. On the next day, the sections were washed and incubated with the secondary antibody for 30 minutes at room temperature. Finally, the slides were developed using a DAB chromogen kit and counterstained with Mayer's hematoxylin.

The total SSH3 immunostaining score was calculated as the sum of the percentage positivity of stained tumor cells and the staining intensity. The percentage positivity was scored from 0 to 3, with 0 for < 10%, 1 for 10-30%, 2 for 31-50%, and 3 for > 50%. The staining intensity was scored from 0 to 3, with 0 for no staining, 1 for weakly stained, 2 for moderately stained, and 3 for strongly stained. Both the percentage positivity of cells and staining intensity were determined in a double-blinded manner. Subsequently, SSH3 expression was calculated as the value of percentage positivity score × staining intensity score, which ranged from 0 to 9. The final expression level of SSH3 was defined as 'low' (0-4) and 'high' (5-9).

Transwell assay

A Boyden chamber with 8-μm-pore filter membrane was used for the in vitro migration assay. Briefly, cells (5×10^4) in culture medium containing 1% fetal bovine serum were seeded in the upper chamber, and culture medium with 10% fetal bovine serum was added in the lower chamber as a chemoattractant. Cells that migrated to the lower surface of the filter were fixed in 4% paraformaldehyde and stained with Giemsa. The migratory cells were counted (10 random 200 × fields per well). Three independent experiments were performed and the data were presented as the mean ± s.e.m.

Wound healing assay

Cells were allowed to grow to confluence, and the monolayer was scratched with a 100 μl pipette tip. The remigration of cells to close the wound was assessed by live cell imaging. The percentage of open area was measured with the software at defined time points (0 and 48 h).

Table S1. Primer sequences used for qRT-PCR (5' to 3')

Gene	Forward primer	Reverse primer
SSH3	TCCAGGTATTGCACCAAGC	GCCATAGCCGTCCACTCAT
GAPDH	GGUGACUAUUCAACCGCAUTT	AUGCGGUUGAAUAGUCACCTT

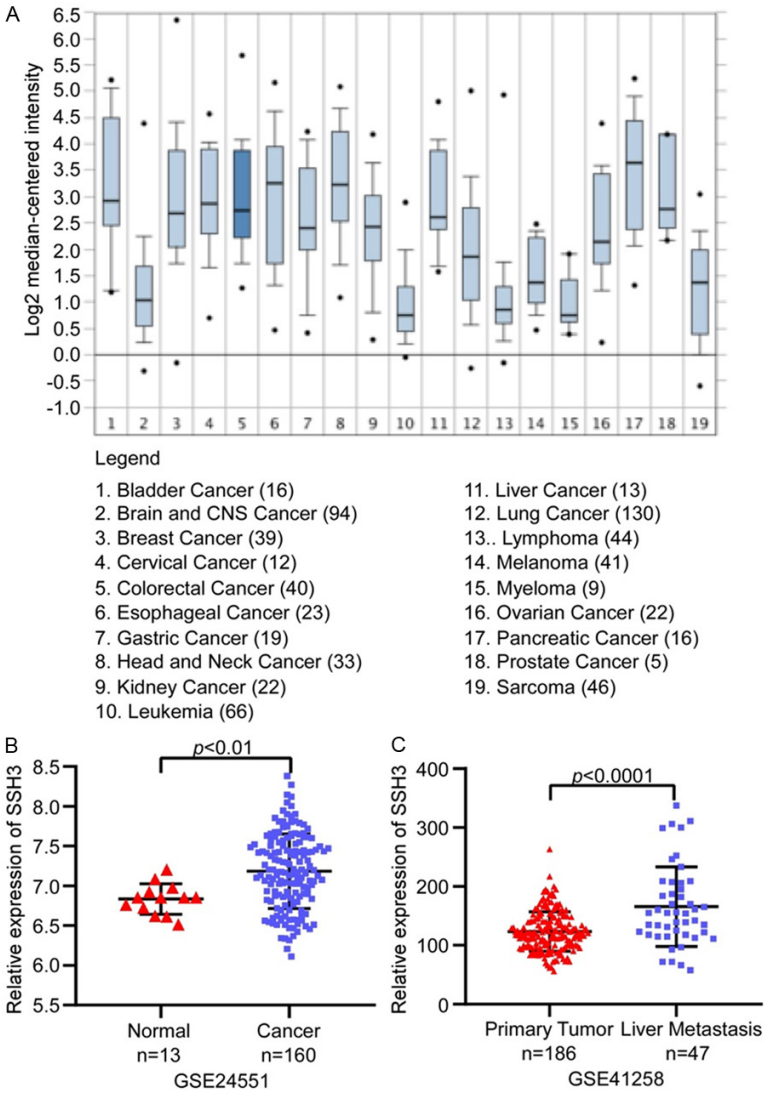

Figure S1. Expression of SSH3 in tumors. A. The analyses of SSH3 expression in various types of tumors by using the public database Oncomine (https://www.oncomine.org/resource/login.html). B. The analyses of SSH3 expression in CRC by using GEO dataset (GSE24551). C. The analyses of SSH3 expression in CRC by using GEO dataset (GSE41258).

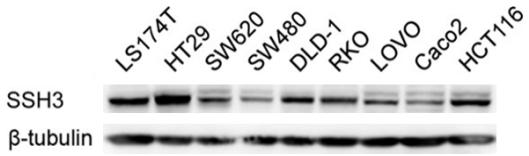

Figure S2. Expression of SSH3 in CRC cells. The expression of SSH3 in different types of CRC cells using Western blot. β-tubulin was used as a loading control.

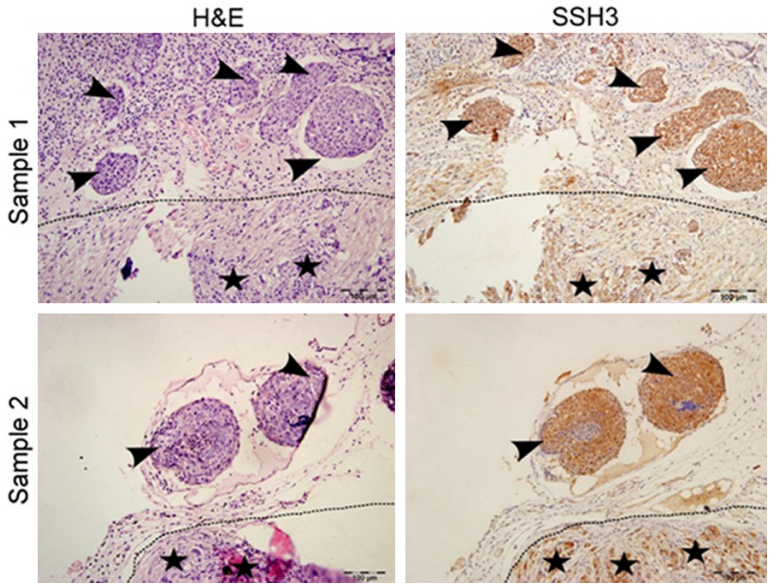

Figure S3. Expression of SSH3 in the primary tumor and the tumor thrombus of the orthotopic mice. SSH3 expression was tested in the primary tumor and the tumor thrombosis of the orthotopic mice using IHC.

A

Query protein	Q8TE77
Gene names	SSH3 SSH3L
Protein name	Protein phosphatase Slingshot homolog 3
Function	Protein phosphatase which may play a role in the regulation of actin filament dynamics. Can dephosphorylate and activate the actin binding/depolymerizing factor cofilin, which subsequently ... view more

Statistics

High confidence predictions (Score>0.5): 61

All predictions (Score>0.1): 139

Interactions in database: 3

Interactor	Gene names	Organism	Prediction code	Prediction LR	Database LR	Final prob.
P53667	LIMK1 LIMK	human	S T G E M C P	17.9	1802.0	0.98

B

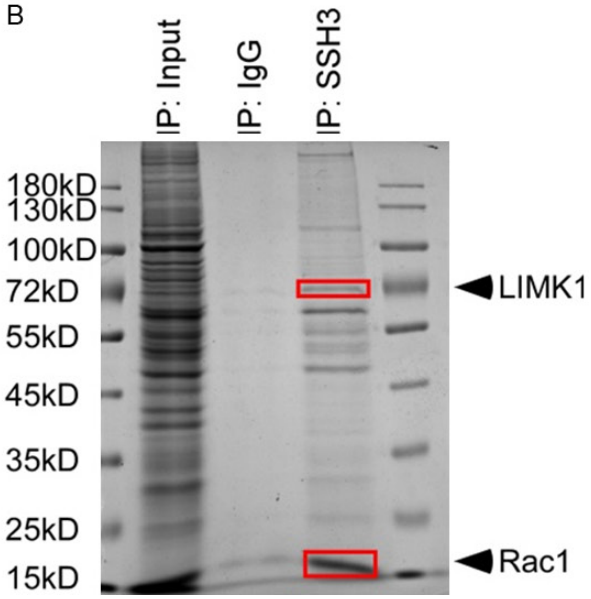

C

Accession number in the database	Score	Mass	Number of matching secondary spectrum	Number of matching peptides	Protein abundances
LIMK1_HUMAN	219	71815	10 (5)	8 (4)	0.21
RAC1_HUMAN	349	21835	16 (15)	10 (10)	6.37

Figure S4. Candidate proteins interacted with SSH3. A. Candidate proteins interacted with SSH3 using the public database PrePPI. B and C. Candidate proteins interacted with SSH3 using the mass spectrometry (MS).